Dasatinib Plus Quercetin Alleviates Choroid Neovascularization by Reducing the Cellular Senescence Burden in the RPE–Choroid

Yinhao Wang,[1–3] Yulin Tseng,[2,3] Keyu Chen,[4] Kuangqi Chen,[1] Kai Chen,[5] Zhihua Huang,[4] Zebin Mao,[4] and Xuemin Li[2,3]

[1]Department of Ophthalmology, First Affiliated Hospital, Zhejiang University School of Medicine, China
[2]Department of Ophthalmology, Peking University Third Hospital, China
[3]Beijing Key Laboratory of Restoration of Damaged Ocular Nerve, Peking University Third Hospital, Beijing, China
[4]Department of Biochemistry and Molecular Biology, Health Science Center, Peking University, China
[5]Department of General Surgery, Peking University First Hospital, Beijing, China

Correspondence: Zebin Mao, Department of Biochemistry and Molecular Biology, Health Science Center, Peking University, No. 38, Xueyuan Road, Haidian District, Beijing 100191, China; zbmao@bjmu.edu.cn.
Xuemin Li, Department of Ophthalmology, Peking University Third Hospital, No. 49, Garden North Road, Haidian District, Beijing 100191, China; lxmlxm66@sina.com.

YW and YT contributed equally to this study.

PURPOSE. Wet AMD (wAMD) is associated with cellular senescence. However, senescent cell–targeted therapies for wAMD have rarely been comprehensively studied. This study aimed to explore the therapeutic effects of senolytic agents on choroidal neovascularization (CNV).

METHODS. RNA sequencing datasets were obtained from the Gene Expression Omnibus database and used to explore the association between senescence and wAMD. We explored the effects of senescent adult RPE cell line-19 cells on the proliferation, migration, invasion, and tube formation of human umbilical vein endothelial cells. A laser-induced CNV animal model was used to study wAMD. We studied a senescent cell elimination therapy for CNV progression using two types of senolytics and a transgenic method.

RESULTS. Cells in the retinal pigment epithelium-choroid of the CNV model were enriched in senescence, inflammation, and angiogenesis gene sets. AP20187 was used to specifically eliminate senescent cells and proven to alleviate CNV progression in *INK-ATTAC* transgenic mice. Senescent adult RPE cell line-1 cells produced elevated levels of senescence-associated secretory phenotypes, including VEGFs; they also demonstrated increased proliferation, migration, invasion, and tube formation in human umbilical vein endothelial cells. The number of senescent cells increased in the laser-induced CNV rat model, and intravitreal injections of dasatinib with quercetin reduced the expression of p16 in CNV and alleviated neovascularization.

CONCLUSIONS. Senescent RPE cells can accelerate pathological neovascularization; thus, senescent cell-targeting therapy has great clinical potential for wAMD.

Keywords: senescence, age-related macular degeneration, senolytic, angiogenesis, choroid neovascularization

AMD—clinically divided into dry (atrophic and nonexudative) and wet (exudative) AMD (wAMD)—is the leading cause of severe vision loss in the elderly.[1,2] Characterized by macular neovascularization, wAMD mainly derives from the choroid (also referred to as choroidal neovascularization [CNV]) and significantly impairs patients' vision. Currently, intravitreal injection of drugs against VEGF—including ranibizumab, bevacizumab, aflibercept, and brolucizumab—is the standard treatment for wAMD.[3] However, more than one-half of patients with wAMD exhibit an incomplete response, even when receiving regular, ongoing anti-VEGF therapy.[4] Increasing studies have described the association between senescent retinal RPE cells and AMD, providing an emerging treatment choice for AMD.[5,6] A previous study demonstrated that nutlin3a, a senolytic drug, could suppress CNV by reducing the senescent cell burden[7]; however, nutlin3a was reported to cause cell senescence,[8,9] making the therapeutic efficacy concerning.

Cellular senescence is an irreversible state of cell growth arrest.[10] Excluding a reduction in replication capacity, senescent cells present significantly altered morphology, gene expression, metabolism, and epigenetic features, and have evolved in multiple biological processes.[11] With the accumulation of senescent cells, organisms age gradually, resulting in various age-related diseases.[11] Senescent cells have been detected in the retina and retinal pigment epitheliums of older humans and primates.[12,13] Additionally, RPE cells present senescent characteristics in laser-induced CNV mouse models.[7] Therefore, strategies targeting senescent RPE cells have been considered novel therapeutic approaches for treating AMD.

Recently, a set of drugs called senolytics were shown to specifically eliminate senescent cells, avoiding nonsenescent

cells.[14] Senolytics have been used to treat various age-related diseases by reducing senescence burden.[7,15,16] Senescence-associated secretory phenotypes (SASPs) are involved in angiogenesis[17]; thus, we hypothesized that the presence of senescent RPE cells is one of the causes of CNV in wAMD. We aimed to validate the association between senescence and AMD using bioinformatics analysis and explore the proangiogenic capacity of senescent RPE cells in vitro. Additionally, we investigated the therapeutic efficacy of various senolytics and a transgenic in vivo approach to reduce the senescence burden on CNV progression.

MATERIALS AND METHODS

RNA Sequencing (RNA-Seq) Datasets From Open Databases

RNA-seq datasets were downloaded from the Gene Expression Omnibus database. The accession numbers and general characteristics of the specimens are summarized in Figure 1B.

Differential Gene Expression (DGE) Analysis

The Limma R package was used for DGE analysis of laser-induced CNV versus controls. Genes with a fold change of >1.5 and a P value of <0.05 were considered differentially expressed genes (DEGs). Volcano plots, generated by Sangerbox 3.0 (http://vip.sangerbox.com/login.html), were used to visualize the DGE analysis.

Gene Set Enrichment Analysis (GSEA)

GSEA was performed on the bulk RNA-seq dataset of protein-coding genes in laser-induced CNV versus controls using 1000 permutations. GSEA (v4.2.2) and Sangerbox 3.0 were used for the analysis. The results were regarded as significant with a normalized enrichment score of >1.0, a P value of < 0.05, and a false discovery rate of <0.25.

Cell Culture and Induction of Cellular Senescence

Adult RPE cell line-19 (ARPE-19) cells were obtained from (Procell Life Science & Technology Co., Ltd., Wuhan, China), and cultured in Dulbecco's modified Eagle's medium (DMEM; TransGen Biotech Co., Ltd., Beijing, China) supplemented with 10% fetal bovine serum (FBS; TransGen Biotech Co., Ltd.), penicillin/streptomycin. Human umbilical vein endothelial cells (HUVECs) were purchased from PharmLab (China) and cultured in ECM (ScienCell Research Laboratories, Carlsbad, CA, USA). Cells were cultured in a humidified incubator with 5% CO_2 at 37°C. ARPE-19 cells and HUVECs at passages 5 through 15 and 5 through 12, respectively, were used in the experiments.

Bleomycin and ionizing radiation (IR) were used to induce senescence in ARPE-19 cells. Cells were treated with 5 µg/mL, 10 µg/mL, 20 µg/mL, and 50 µg/mL bleomycin for 24 hours, and subsequently incubated in bleomycin-free 10% FBS DMEM, which was replaced every 2 to 3 days. The cells were treated with IR (4.125 Gy/min) for 145 seconds for a total dose of 10 Gy. The cells were then cultured in 10% FBS DMEM, which was replaced every 2 to 3 days. After 5 or 7 days, bleomycin- or IR-induced senescent ARPE-19 cells and young ARPE-19 cells were used for further experiments.

SA-β Gal Staining

SA-β gal staining was performed following the instruction of the SA-β gal staining kit (Beyotime Biotechnology, Shanghai, China). Briefly, the cells were seeded in 24-well plates and senescence was induced. The cells were fixed with fixation solution for 15 minutes at room temperature, washed with PBS, stained with staining solution for 8 hours in a CO_2-free incubator at 37°C, and, finally, washed with PBS. Images were captured using an inverted microscope.

Protein Extraction and Western Blotting

ARPE-19 cells grown in 10-cm culture dishes were lysed in RIPA buffer (Beyotime Biotechnology, China) supplemented with a protease inhibitor cocktail (Bimake, Houston, TX, USA). The protein concentration was quantified using the Bradford assay. Equal amounts of protein were loaded onto the running lanes, which were separated by SDS-PAGE in 12% polyacrylamide gel, and transferred onto polyvinylidene difluoride membranes. The polyvinylidene difluoride membrane was blocked with skim milk for 1 hour at room temperature, and subsequently incubated overnight at 4°C with primary antibodies (Supplementary Table S2). After washing with TBST, the membranes were incubated with secondary antibodies (Supplementary Table S2) for 1 hour at room temperature, and visualized using BeyoECL Plus (Beyotime Biotechnology).

RNA Isolation and Real-Time Quantitative PCR (qPCR)

All reagents and consumables used for RNA extraction were RNase free. Total RNA was extracted from ARPE-19 cells cultured in 6-cm culture dishes using TRIzol reagent (Life Technologies, Carlsbad, CA, USA). The quantification of RNA was performed using a nanodrop, and only RNA samples with an $OD_{260}/OD_{280} = 1.9$–2.1 and $OD_{260}/OD_{230} = 2.0$–2.4 were used for further analyses. The RNA integrity numbers were 8 to 10. Reverse transcription was conducted using the ReverTra Ace qPCR RT kit (Toyobo, Osaka, Japan) including a 20-µL mix system with 2 µg RNA (37.0°C for 30 minutes, 95.0°C for 5 minutes) following the manufacturer's instructions. Reverse transcription was performed in 200-µL tubes (Wuxi NEST Biotechnology Co., Ltd., Jiangsu, China). The cDNA was preserved at 4°C before real-time qPCR.

The cDNA samples were amplified with specific primers using the qPCR SYBR Green Master Mix (Yeasen Biotechnology Co., Ltd., Shanghai, China) on a 7500 Real-Time PCR System (Applied Biosystems, Waltham, MA, USA). Real-time qPCR was conducted using a 20-µL mix system, and the program was set as follows: holding stage (95.0°C for 3 minutes), cycling stage (95.0°C for 10 seconds, and 60.0°C for 30 seconds; 40 cycles), and melt curve stage (95.0°C for 15 seconds, 60.0°C for 1 minutes, 95.0°C for 30 seconds, and 60.0°C for 15 seconds). The relative mRNA expression was calculated using the $2^{-\triangle\triangle Ct}$ method, and mean Ct values were normalized to those of GAPDH. Real-time PCR was performed in triplicate for each group. The primer sequences are listed in Supplementary Table S1.

Conditioned Media (CM) Collection

After 5 days of inducing senescence, ARPE-19 cells were used to collect CM. Senescent and young ARPE-19 cells
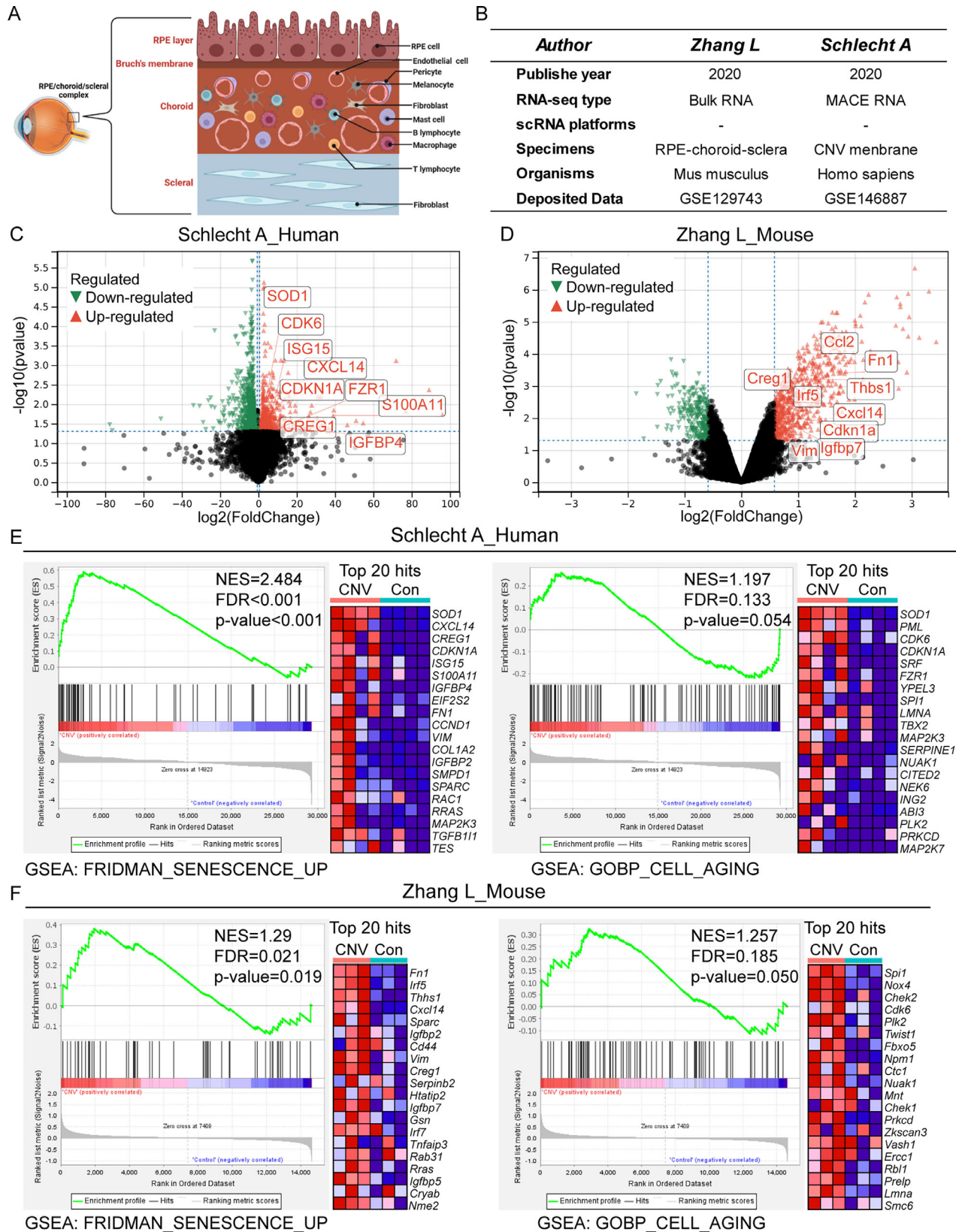
FIGURE 1. Cells in the RPE–choroid complex exhibited enrichment of senescence-associated genes based on the human (GSE146887) or mouse (GSE129743) CNV datasets from the Gene Expression Omnibus (GEO) database. (**A**) Schematic of RPE-choroidal cell types (created with BioRender.com, agreement number: YP25RVP6Q9). (**B**) Basic information of RNA-seq datasets. (**C–D**) Volcano plots showing the DEGs in patients with wAMD (**C**) and mouse CNV models (**D**) versus controls. _Red dots_ represent upregulated genes, while green points represent downregulated genes. Genes with a fold change >1.5 and a _P_ value of <0.05 were considered DEGs. (**E–F**) GSEA enrichment plots illustrating

gene sets involved in senescence in patients with wAMD (**E**) and mouse CNV models (**F**). The enrichment was regarded as significant with an NES of >1.0, a *P* value of <0.05, and a false discovery rate of <0.25. DEG, differentially expressed gene; NES, normalized enrichment score; wAMD, wet AMD.

were cultured in 10-cm culture dishes. Cells were washed with PBS twice, and further cultured in complete DMEM for 48 hours. Following incubation, CM were centrifuged at $2000 \times g$ for 10 minutes to remove cells and cell debris, and then stored in aliquots at −80°C until use. The CM underwent one or two freeze–thawing cycles before use.

Cell Viability Assay

In vitro HUVEC proliferation was measured using a Cell Counting Kit-8 (DOJINDO Laboratories, Kumamoto, Japan). Following the manufacturer's instructions, 4000 cells/well were seeded in a 96-well plate with a final volume of 100 µL CMs or complete DMEM. Culture media were replaced with 100 µL serum-free DMEM at different time points, and Cell Counting Kit-8 solution (10 µL) was added to each well. The absorbances at 450 nm and 630 nm were measured after incubation for 1 hour at 37°C, and the number of viable cells were calculated as $OD_{450} - OD_{630}$.

Migration and Invasion Assay

Migration assays were performed using Transwell filter chambers (Corning Inc., Corning, NY, USA). Transwell filter chambers coated with Matrigel (Corning Inc.) were used for invasion assays. For CM, HUVECs (2×10^4 for migration, 4×10^4 for invasion) in 200 µL serum-free DMEM were seeded in the upper chamber; 600 µL CM or complete DMEM were simultaneously added to the lower chamber. For coculture, young or senescent (5 days after senescence induction) ARPE-19 cells were seeded into the lower chamber. A total of 2×10^4 (migration) or 4×10^4 (invasion) HUVECs in 200 µL serum-free DMEM were seeded in the upper chamber; the medium in the lower chamber was replaced with 600 µL complete DMEM 1 day ahead. After incubation in a humidified incubator at 37°C for 24 hours, cells were fixed with 4% paraformaldehyde (Beijing Solarbio Science & Technology Co., Ltd., Beijing, China) and stained with 0.1% crystal violet (Beijing Solarbio Science & Technology Co., Ltd.). Five images from each well were randomly captured to determine the number of cells that migrated through the membrane. Each assay was performed in triplicate.

Tube Formation Assay

A prechilled 96-well plate was coated with 50 µL Matrigel (Corning Inc.) and incubated for 30 minutes at 37°C. The HUVECs (2×10^4) in 50 µL of various CM were seeded in a 96-well plate. After 3 hours of incubation at 37°C, the EC tubular structure had formed. The tube area of 3 random fields per well was photographed using an inverted microscope (IX73; Olympus Corporation, Tokyo, Japan).

Flow Cytometry Analysis for Apoptosis

Flow cytometry analysis for apoptosis was performed according to the manufacturer's instructions using an apoptosis test kit (KeyGEN BioTECH Corp., Ltd., Nanjing, China). Briefly, adherent cells were collected, washed with PBS, and

resuspended in the binding buffer. Cells were stained with Annexin V-APC and propidium iodide, and counted by flow cytometry using FolJo version 10 to analyze the data.

TUNEL Assay

The one-step apoptosis assay kit (Beyotime Biotechnology, China) was used to detect apoptosis according to the manufacturer's instructions. In brief, young and senescent ARPE-19 cells were fixed with 4% paraformaldehyde for 30 minutes, washed with PBS, and incubated with 0.5% Triton X-100 at room temperature for 5 minutes. After washed with PBS twice, the fixed cells were incubated in 50 µL reaction mixture for 60 minutes in the dark. Stained cells were washed three times with PBS and mounted with an antifading mounting medium (DAPI; Beijing Solarbio Science & Technology Co., Ltd.). The stained cells were observed, and images were captured using a confocal laser scanning microscope (FV3000; Olympus Corporation).

Animals

All animal procedures were approved by the Animal Ethics Committee of the Peking University Health Science Center and conducted in accordance with the guidelines of the ARVO in the Statement for the Use of Animals in Ophthalmic and Visual Research. Male Brown Norway (BN) rats (aged 7–8 weeks) were purchased from SPF Biotechnology Co., Ltd. (Beijing, China). *INK-ATTAC* transgenic mice were purchased from GemPharmatech Co., Ltd. (Nanjing, China). The genomes of these mice contained a knock-in fragment encoding the FK506-binding proteincaspase-8 fusion protein, which is controlled by the promoter of *Cdkn2a* (*Ink4a*). AP20187 induces dimerization and activation of caspase-8, and ultimately, apoptosis of p16^{Ink4a}-positive cells. All animals were housed in a specific pathogen-free environment with a 12-hour light/dark cycle at 22 ± 2°C with free access to food and water. Genotyping was performed to validate INK-ATTAC transgenic mice using the Quick Genotyping Assay Kit for mouse tails (Beyotime Biotechnology). The following primers were used:

F1: TCAGCGTTCAGACTCCTCAGAATGT
R1: TTGTAGGGACCCAGATGCAAATC
F2: AACGTGCTGGTTGTTGTGCTGTC
R2: TCACAGAAACCATATGGCGCTCC
F3: CAGCAAAACCTGGCTGTGGATC
R3: ATGAGCCACCATGTGGGTGTC

Laser-Induced CNV Model

BN rats and INK-ATTAC mice were anesthetized, and topical oxybuprocaine (Santen, Osaka, Japan) and tropicamide phenylephrine eye drops (Santen) were administered for local anesthesia and pupil dilation, respectively. An animal model was established using a slit-lamp delivery system equipped with a laser photocoagulator (Vision One; Lumenis, Yokneam, Israel). The laser parameters were set as follows: 532 nm, 300 mW, 0.05 second duration, and 50 µm

spot size (BN rats); 532 nm, 200 mW, 0.05 second duration, and 50 µm spot size (INK-ATTAC mice). Six laser spots for BN rats and three laser spots for INK-ATTAC mice were generated around the optic nerve head using a cover slip. Laser spots that produced bubbling were considered to disrupt the Bruch's membrane, and only these spots were included in the study.

Intravitreal Injection

For the intravitreal injection, we randomly selected one eye from a BN rat for injection with the drugs, and the other eye from the same rat was injected with the vehicle after local anesthesia and pupil dilation. Under a dissection microscope, a 33G sterile needle was inserted into the vitreous cavity, 1 mm away from the limbus. Using a microsyringe (Hamilton Company, Reno, NV, USA), 5 µL of the drug or vehicle was injected into the vitreous cavity; thereafter, the needle was maintained in the vitreous cavity for at least 1 minute to prevent drug leakage. The drug concentrations were as follows: 10 ng/µL dasatinib (LC Laboratories, Woburn, MA, USA) + 50 ng/µL quercetin (Sigma-Aldrich, MO, USA) (6 eyes from 6 male BN rats in each group); 40 ng/µL 17-DMAG (18 eyes from 18 male BN rats); or 2 µg/µL aflibercept (Eylea) (8 eyes from 8 male BN rats in each group).

Intraperitoneal Injection and Oral Gavage

After laser photocoagulation, BN rats were administrated 3.5 mg/kg dasatinib and 35 mg/kg quercetin daily via intraperitoneal injection or oral gavage at specific time points (days 2–5). For each group of BN rats, 6 to 10 eyes of 3 to 5 male BN rats were included in the experiments. INK-ATTAC mice (aged 10–12 weeks, 5 mice per group, including 2 females and 3 males) were treated intraperitoneally injected with 5 mg/kg AP20187 (MedChemExpress, Monmouth Junction, NJ, USA) from day 2 to day 5.

Fundus Assessment

Fundus assessments were performed on days 7 and 14, including fundus photography, infrared photography, and fundus fluorescein angiography (FFA). Fundus images were obtained using a panoramic ophthalmoscope (Daytona-P200T; Optos, Dunfermline, UK), whereas infrared photographs and FFA images were obtained using a scanning laser ophthalmoscope (Heidelberg Eye Version 10.2.0; Heidelberg Engineering, Inc., Heidelberg, Germany). Briefly, BN rats were anesthetized, and their pupils were dilated with tropicamide phenylephrine (Santen) before examination. FFA images were taken at appropriate intervals for 15 minutes after a 2 mL/kg intraperitoneal injection of 10% fluorescein sodium (Alcon, Geneva, Switzerland).

Hematoxylin and Eosin (H&E) Staining

Enucleated eyeballs were fixed in FAS fixative (Wuhan Servicebio Technology Co., Ltd., Wuhan, China), and embedded in paraffin; 5-µm sections were prepared and mounted on slides. After deparaffinization in xylene and rehydration in a decreasing concentration gradient of ethanol, the slides were used for H&E staining, conducted according to the manufacturer's protocol using an H&E Staining Kit (Beyotime Biotechnology, China).

Immunofluorescence of IB4 for RPE–Choroid Flat Mount

The procedure was modified as previously described.[18] The animals were deeply anesthetized and their eyes were immediately enucleated. After 1 hour of fixation with 4% paraformaldehyde (Biorigin, BN20094, China), anterior segments were removed from enucleated eyes; retinal cups were carefully dissected under a dissecting microscope. For costaining of isolectin IB4 and p16, RPE–choroid–sclera complex tissues were washed with cold ICC buffer (0.5% BSA, 0.2% Tween 20, and 0.05% Proclin300 in PBS) and blocked with 1% goat serum for 1 hour at room temperature. The RPE–choroid–sclera complex tissues were subsequently incubated overnight at 4°C with isolectin IB4 (Thermo Fisher Scientific, Waltham, MA, USA) and anti-p16 antibodies (Abcam, Cambridge, UK), washed with cold ICC buffer, and incubated with a goat anti-mouse IgG antibody (EarthOx, Millbrae, CA, USA) at room temperature for 1 hour. Finally, cells were stained with Hoechst 33342 (KeyGEN BioTECH Corp., Ltd.) at 4°C for 15 minutes, washed with PBS, and mounted on slides.

For monostaining of isolectin IB4, RPE–choroid–sclera complex tissues were washed with ICC buffer, incubated with isolectin IB4 overnight at 4°C, stained with Hoechst 33342 for 15 minutes at 4°C, washed with ICC buffer, and mounted on slides. Images were captured using an inverted fluorescence microscope. To measure the CNV lesion area, we drew a circle around the region of interest using the Image-Pro Plus 6.0 software, which automatically masks the CNV lesion and calculates the area. The CNV lesion area percentage was calculated as: CNV area% = CNV area/whole field area.

Multicolor Immunofluorescent Staining

Formalin-fixed paraffin-embedded sections of eye tissues were subjected to multicolor immunofluorescent staining. Briefly, sections were deparaffinized in fresh xylene for 10 minutes twice, and rehydrated in decreasing concentrations of ethanol (100%, 100%, 95%, 90%, 80%, and 70%) for 5 minutes. Antigens were retrieved using a microwave heating method in the presence of EDTA, and cooled for at least 10 to 15 minutes in an ice-water bath. Endogenous peroxidases were removed via incubation with 3% H_2O_2 at room temperature for 25 minutes. Blocking was performed with 3% BSA for 30 minutes at room temperature, followed by incubation with primary antibodies overnight at 4°C, secondary antibodies for 50 minutes at room temperature, and Flare fluorophores for 3 to 5 minutes. Antigen retrieval, blocking, primary antibody and antibody incubation, and flare fluorophore staining were repeated for each marker. Finally, the sections were counterstained with DAPI (Sigma-Aldrich, St. Louis, MO, USA) for 5 minutes, and mounted. The following primary antibodies were used: p21 (Proteintech), p16 (Abcam), RPE65 (Proteintech), and CD31 (Abcam).

Statistical Analysis

All data were presented as mean ± standard deviation. The Student *t* test was used for comparisons between two groups, and ANOVA was used to compare multiple groups (>2). GraphPad Prism version 8 (San Diego, CA, USA) was used

for all analyses; a *P* value of <0.05 was considered significant.

RESULTS

Cells in the RPE–Choroid of Patients With wAMD, or CNV Models, Demonstrated Enrichment of Senescence-Associated Genes

To explore cellular senescence in wAMD, we first analyzed existing RNA-seq datasets (GSE146887 and GSE129743). Specimens were obtained from the RPE-choroid layer (Fig. 1A) of patients with wAMD (GSE146887), CNV mouse models (GSE129743), and corresponding controls. Information regarding the datasets are shown in Figure 1B. First, we performed DGE analysis and found that many senescence-associated genes were upregulated in the CNV (Figs. 1C–D), including *CDKN1A*, *SOD1*, and *S100A11* in humans, and *Cdkn1a*, *Ccl2*, and *Fn1* in mice. GSEA was performed to detect cellular senescence in the RPE–choroid. Compared with the controls, mice with CNV showed enrichment of known senescence-associated gene sets, including FRIDMAN_SENESCENCE_UP and GOBP_CELL_AGING (Figs. 1E–F). Furthermore, we explored the biological processes associated with CNV formation by combining GSEA with the Gene Ontology, Kyoto Encyclopedia of Genes and Genomes, REACTOME, and Wiki pathways. Pathways associated with angiogenesis were significantly activated (Supplementary Figs. S1A–B), and genes associated with inflammation—including complement activation, signaling by interleukins, and chemokine signaling pathways—were enriched (Supplementary Figs. S1C–D). This finding indicates a potential association between cellular senescence, inflammation, and angiogenesis in wAMD. To determine commonalities between mouse CNV and human samples through DGE analyses, we detected 29 commonly upregulated and 10 downregulated DEGs in these two datasets (Supplementary Figs. S2A–B). Based on the common DEGs, common pathways related to human and mouse CNV were enriched through Gene Ontology and Kyoto Encyclopedia of Genes and Genomes enrichment analyses (Supplementary Figs. S2C–F).

AP20187 Significantly Inhibits the Formation of CNV in INK-ATTAC Mice

To validate the role of senescent cells in CNV formation, we determined the therapeutic potential of selectively eliminating these cells and attempted to ablate p16^{Ink4a}-positive cells in *INK-ATTAC* mice.[19] The genomes of these mice contained a knock-in fragment encoding the FK506-binding proteincaspase-8 fusion protein, which is controlled by the promoter of *Cdkn2a* (*Ink4a*). AP20187 induced the dimerization and activation of caspase-8 and, ultimately, the apoptosis of p16^{Ink4a}-positive cells (Fig. 2A). After genotype identification (Fig. 2B), *INK-ATTAC* mice were used to establish a CNV model using a 532-nm wavelength laser (Fig. 2C). FFA, H&E staining, and IB4 immunofluorescence staining of the RPE–choroid mount showed that a laser-induced CNV mouse model was successfully established (Figs. 2D–F). Additionally, p16 immunofluorescence staining of the RPE–choroid mount validated the increase in senescent cells in the RPE–choroid tissues of CNV mice (Fig. 2F). Thereafter, *INK-ATTAC* mice were administered AP20187 or vehicle (Fig. 2G). Intraperitoneal injections of AP20187 in laser-induced CNV mice led to a more than 2.0-fold decrease in pathological neovascularization on day 7 (Fig. 2H), further validating the rationale for therapeutically targeting senescent cells in CNV.

Inducing Senescent ARPE-19 Cells

RPE cells play an important role in AMD progression; thus, they were cultured for further investigation.[3] Based on previously reported methods,[20,21] we induced senescence in ARPE-19 cells using bleomycin and IR. To determine suitable experimental conditions, we prepared a series of bleomycin concentrations: 5 µg/mL (B5), 10 µg/mL (B10), 20 µg/mL (B20), and 50 µg/mL (B50). After 7 days of incubation, ARPE-19 cells became larger and irregular, with a significantly increased number of β-gal$^+$ cells (Figs. 3A–B). Cell viability gradually decreased with increasing bleomycin concentrations (Fig. 3C).

Next, we evaluated the expression of senescence markers in ARPE-19 cells. The mRNA and protein expression levels of p16, p21, and p53 were upregulated in the B10 and IR groups 5 and 7 days after induction (Figs. 3D–F). SASPs, a key feature of cellular senescence, involves a set of proinflammatory mediators, such as cytokines, chemokines, and matrix metalloproteinases (MMPs).[22] We observed that SASPs significantly increased after 5- or 7-day treatments with bleomycin and IR (Fig. 3G and Supplementary Fig. S3). Interestingly, we noticed that TNF-α was significantly upregulated on day 5, and significantly reduced on day 7, reflecting the dynamic changes of SASPs. Because the percentage of β-gal$^+$ cells was highest in B10, this concentration was selected for subsequent experiments.

Senescent ARPE-19 Cells Prompted the Proliferation, Migration, Invasion, and Tube Formation of HUVECs

VEGF was significantly upregulated in senescent ARPE-19 cells (Fig. 3G and Supplementary Fig. S3); thus, we explored the effect of senescent ARPE-19 cells on angiogenesis. We observed that CM from senescent APRE-19 cells significantly promoted HUVEC proliferation (Fig. 4A). In wAMD, CNV breaks through Bruch's membrane into the retina, which relies on the migration and invasion capabilities of vascular ECs. We investigated the effect of senescent ARPE-19 cells on the migration and invasion of HUVECs (Fig. 4B). By coculturing HUVECs with ARPE-19 cells, or treating HUVECs with CM, we found that both ARPE-19 cells and CM promoted the migration of HUVECs (Figs. 4C–D). The invasion of HUVECs was accelerated by senescent ARPE-19 cells (Figs. 4E–F). Additionally, we noticed that young ARPE-19 cells showed slightly improved migration and invasion compared with negative controls (Figs. 5C–F), which were inferior to those of senescent ARPE-19 cells. Finally, a tube formation assay was performed; the number and size of tube lumens increased after treatment with B10 or IR CM for 3 hours (Fig. 4G). These results indicate that senescent ARPE-19 cells have a positive effect on angiogenesis.

Senolytics Specifically Induced Senescent ARPE-19 Cell Death

Senolytics are drugs that specifically kill senescent cells without destroying young cells.[14] Dasatinib plus quercetin
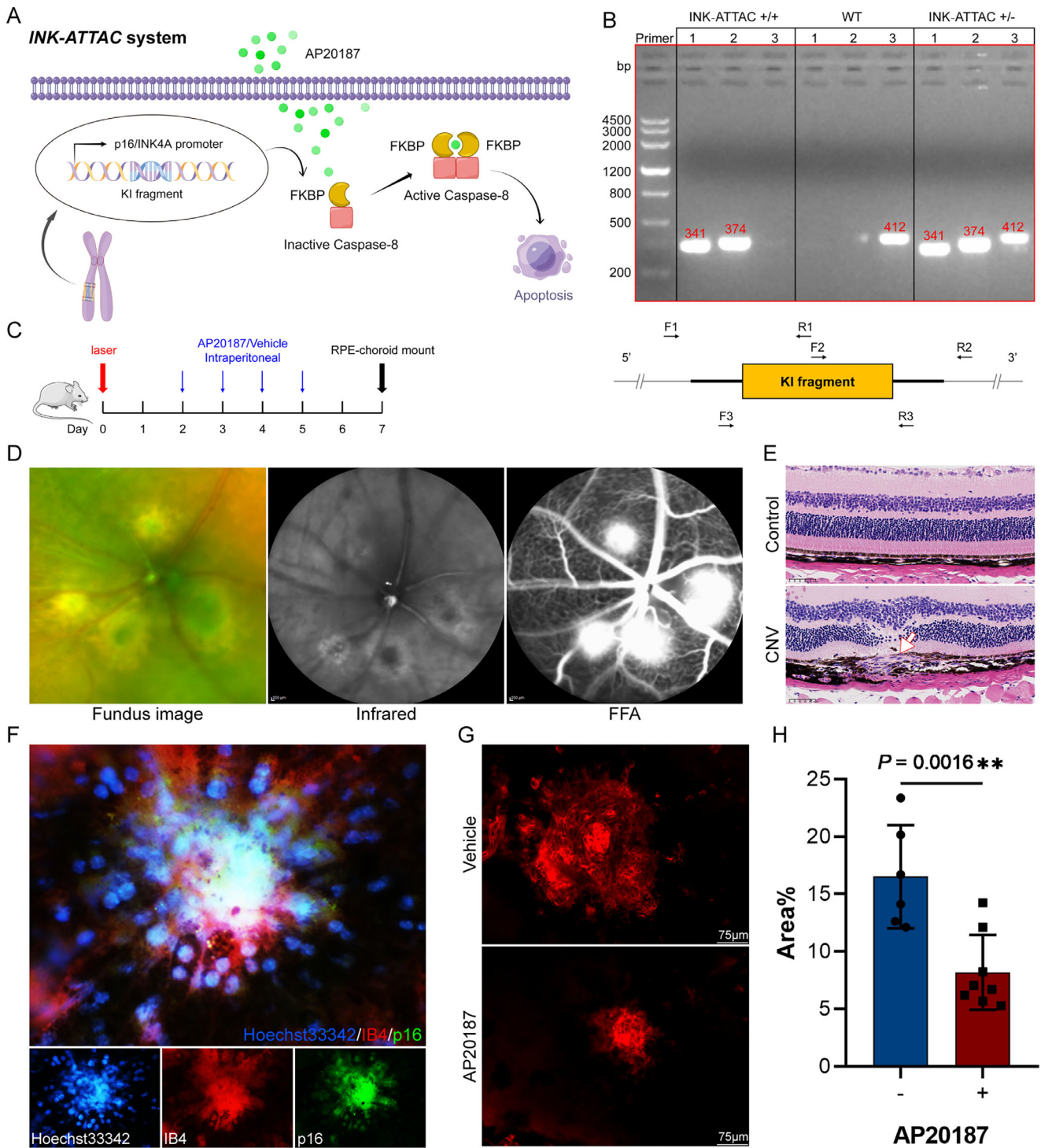
FIGURE 2. Specifically eliminating senescent cells in *INK-ATTAC* mice significantly reduced the size of CNV. (**A**) Schematic diagram showing the *INK-ATTAC* system (by Figdraw). (**B**) Genotype identification for the *INK-ATTAC* mice. Two bands were seen in *INK-ATTAC*^{+/+} mice, three bands were seen in *INK-ATTAC*^{+/−}, mice and only one band was seen in WT mice. (**C**) Flowchart for treatment of AP20187 to laser-induced CNV *INK-ATTAC* mouse model. (**D**) Fundus image, infrared photo, and FFA image of the CNV *INK-ATTAC* mouse model. (**E**) H&E staining of the normal and CNV *INK-ATTAC* mouse model. (**F**) Immunofluorescence staining of IB4 and p16 for the RPE–choroid–scleral complex mount in CNV *INK-ATTAC* mouse model. (**G–H**) Immunofluorescence of the RPE–choroid–sclera complex showing that AP20187 significantly alleviated the progression of CNV in *INK-ATTAC* mice ($n = 6$ without vs. $n = 8$ with AP20187; each datapoint represents the average value of the lesions from 1 eye). **$P < 0.01$. The Student t test was used for comparisons between the two groups. WT, wild-type.

(D+Q) and 17-DMAG are different types of senolytics that selectively eliminate senescent cells.[23,24] To explore the sensitivity of ARPE-19 cells to senolytics, we incubated the ARPE-19 cells with the two senolytics. First, we conducted a TUNEL assay and found that TUNEL^{+} senescent cells increased after 24 hours incubation with D+Q (Fig. 5A).
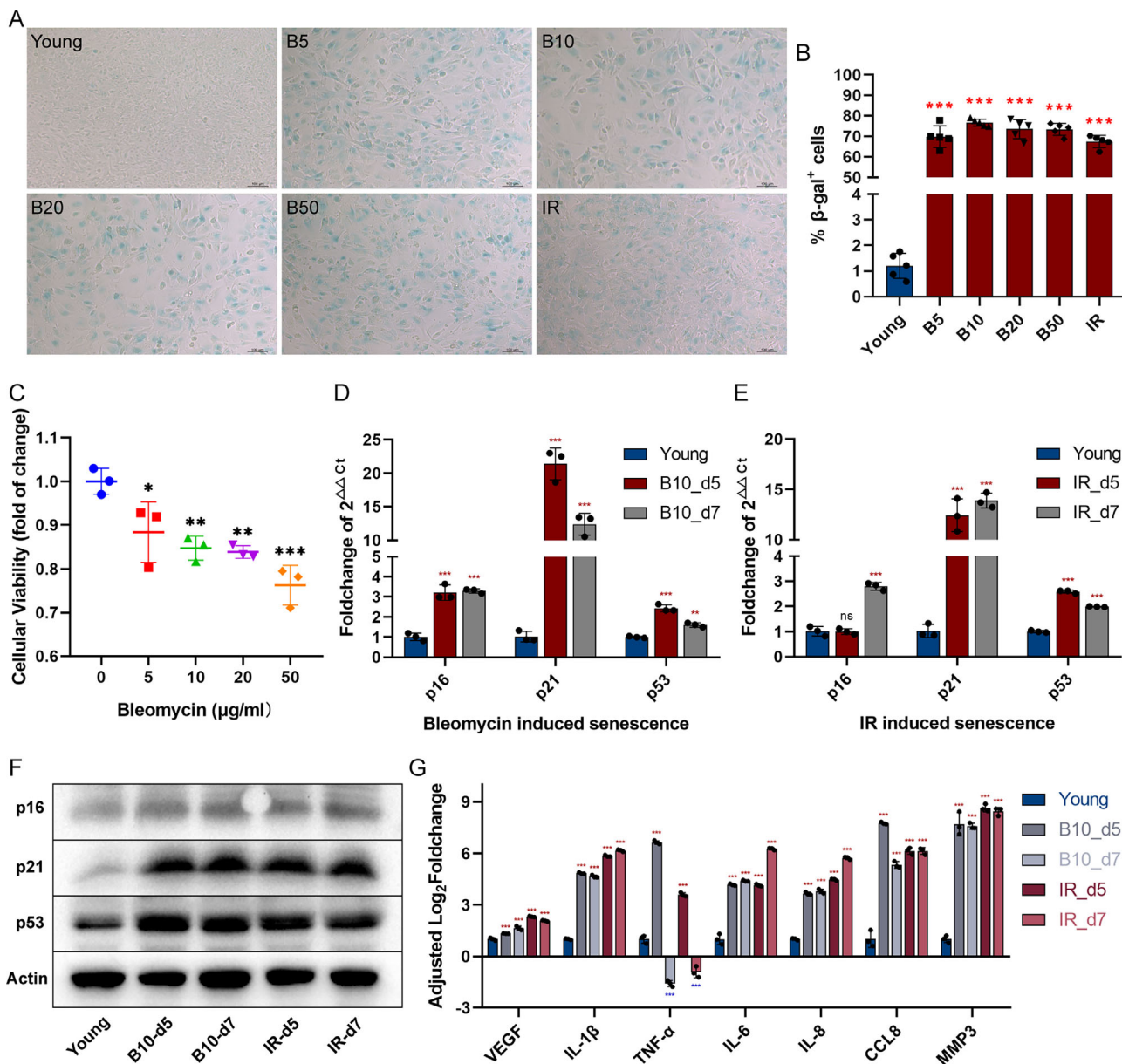
FIGURE 3. Induction of senescent ARPE-19 cells. (**A**) SA-β-gal staining of senescent and young ARPE-19 cells. The *blue area* represents positive SA-β-gal staining, indicating senescence; B. Proportions of β-gal$^+$ cells in different groups. (**C**) Cell viability of ARPE-19 after 24 h of treatment with bleomycin at different concentrations. (**D–E**) Real-time PCR showing the mRNA expression level of p53, p21, and p16 on days 5 and 7. (**F**) Western blot showing the protein expression of p53, p21, and p16. (**G**) Real-time PCR showing the mRNA expression level of SASPs on days 5 and 7. B5, 5 µg/mL bleomycin; B10, 10 µg/mL bleomycin; B20, 20 µg/mL bleomycin; B50, 50 µg/mL bleomycin. *$P <$ 0.05; **$P <$ 0.01; ***$P <$ 0.001. One-way ANOVA was used for comparisons among groups. All experiments were performed in triplicate (at least).

However, the number of TUNEL$^+$ senescent cells did not increase obviously after 24 hours incubation with 17-DMAG, indicating that senescent ARPE-19 cells were more sensitive to D+Q. Flow cytometry showed that young ARPE-19 cells survived D+Q treatment (Figs. 5B–E, and Supplementary Figs. S4A–D); however, the number of apoptotic senescent ARPE-19 cells greatly increased after 48 hours of treatment with D+Q (Supplementary Figs. S4A–D). After 72 hours, this increase in apoptotic senescent ARPE-19 cells became more obvious (Figs. 5B–E). After incubation with 17-DMAG, young ARPE-19 cells did not demonstrate significant apoptosis (Figs. 5B–E and Supplementary Figs. S4B–E); apoptosis increased after 72 hours, which was later than observed after

treatment with D+Q (Figs. 5B–E). Considering the timing and rate of apoptosis, senescent ARPE-19 cells were more sensitive to D+Q than 17-DMAG.

We explored apoptotic mechanisms of senescent ARPE-19 cells after treatment with senolytics. Western blotting was used to analyze the protein levels of cleaved caspase-3 and Bcl-2/Bax in bleomycin-induced senescent ARPE-19 cells. Additionally, we tested other death mechanisms, including autophagy (p62), necroptosis (pMLKL/MLKL), pyroptosis (caspase-1), and ferroptosis (GPX4; Supplementary Figs. S5A–H). We observed that Bcl-2 expression significantly decreased with increased Bax expression in D+Q–treated senescent ARPE-19 cells (Supplementary Figs. S5A, E, F).
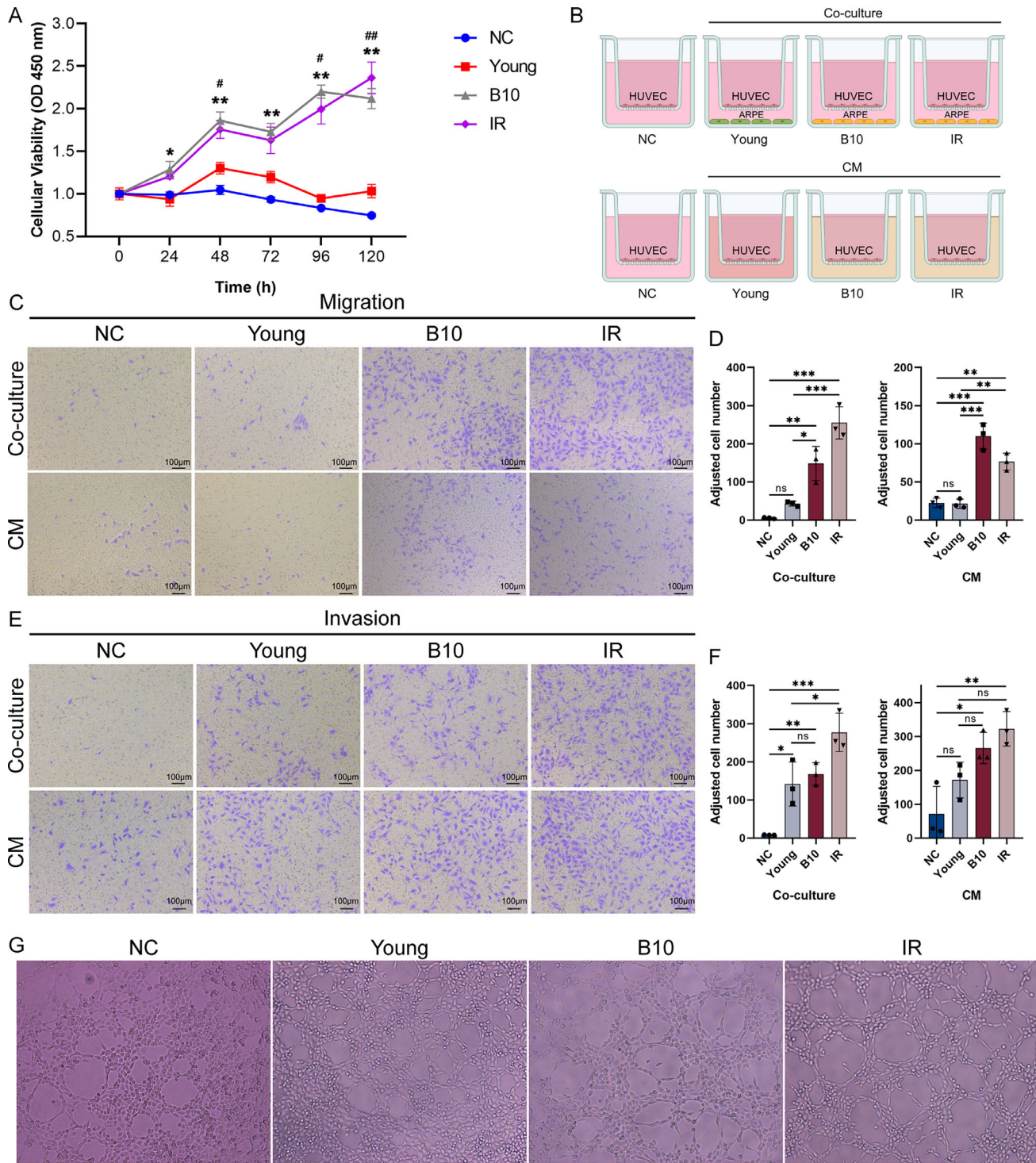
Figure 4. Senescent ARPE-19 cells promote the proliferation, migration, invasion, and tube formation of HUVECs. (**A**). Cell Counting Kit-8 results demonstrating the proliferation of HUVECs after treatment with different CM. *B10 vs. young; #IR vs. young. The experiments were performed in triplicate for analysis; two-way ANOVA was used for comparisons among groups. (**B**) Schematic diagram of migration and invasion assay for HUVECs (created with BioRender.com; agreement number: FS255J17FA). (*Top*) Coculture of HUVECs and ARPE-19 cells. (*Bottom*) Culture of HUVECs with CM. (**C–D**) Senescent ARPE-19 cells facilitate the migration of HUVECs. The experiments were performed at least in triplicate for analysis. One-way ANOVA was used was used for comparisons between the two groups. (**E–F**) Senescent ARPE-19 cells facilitate the invasion of HUVECs. The experiments were performed at least in triplicate for analysis. One-way ANOVA was used for comparisons between the two groups. (**G**) CM from senescent ARPE-19 cells promote tube formation in HUVECs. Compared with CM from young ARPE-19 cells, larger lumen sizes and more tube rings formed after HUVECs were cocultured with the CM of senescent ARPE-19 cells for 4 hours on Matrigel. B10, 10 µg/mL bleomycin; NC, negative control; Ns, not significant. * (#)$P < 0.05$; ** (##)$P < 0.01$
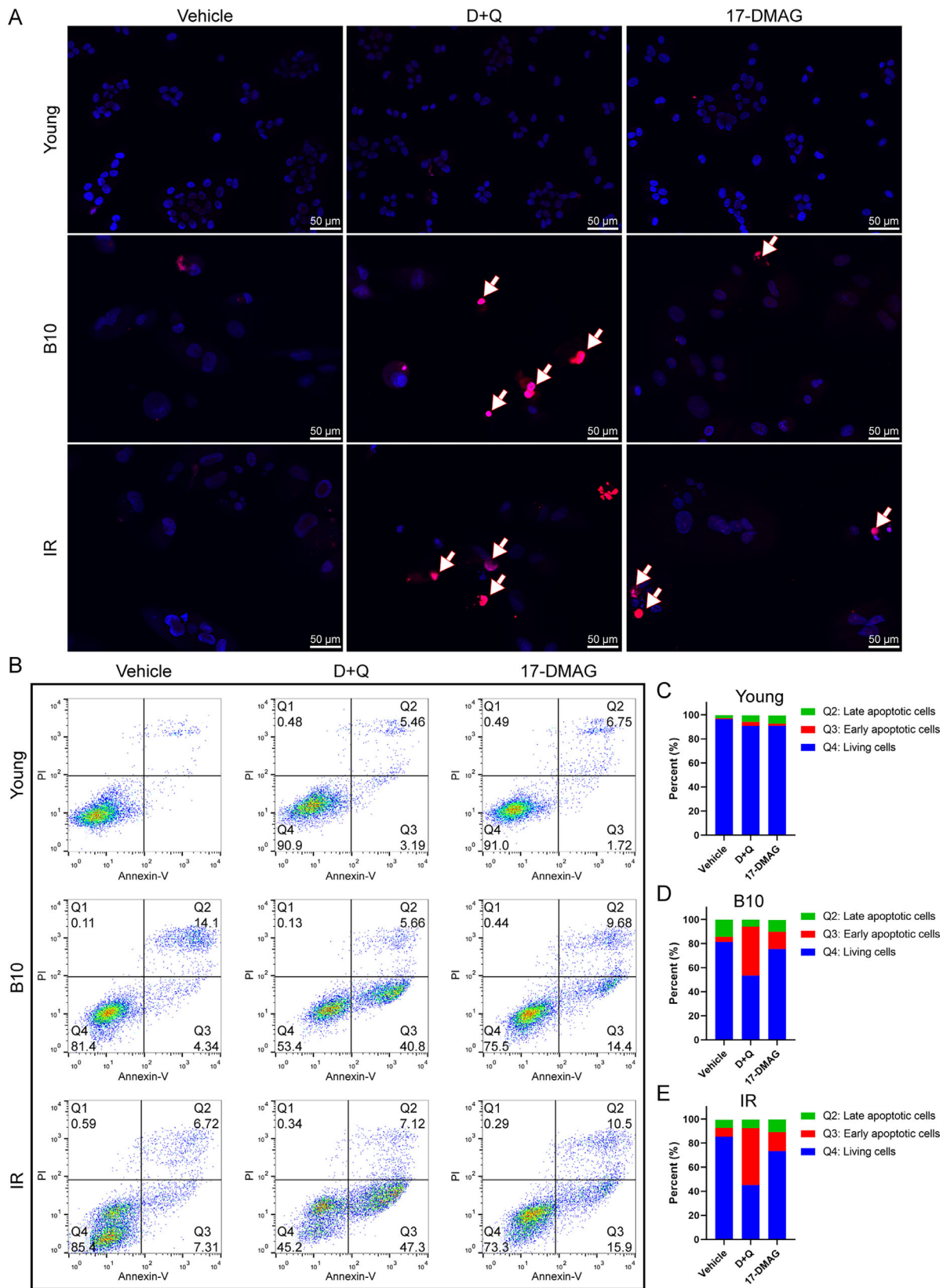
FIGURE 5. Proapoptosis effect of senolytics on senescent ARPE-19 cells. (**A**) TUNEL staining of young and senescent ARPE-19 cells after 24 h of treatment with the vehicle, D+Q, or 17-DMAG. The *arrows* indicate TUNEL^{+} cells. (**B**) Flow cytometry results of apoptotic ARPE-19 cells after 72 h of treatment with the vehicle, D+Q, or 17-DMAG. (**C–E**) Proportion of apoptotic and living ARPE-19 cells based on flow cytometry.
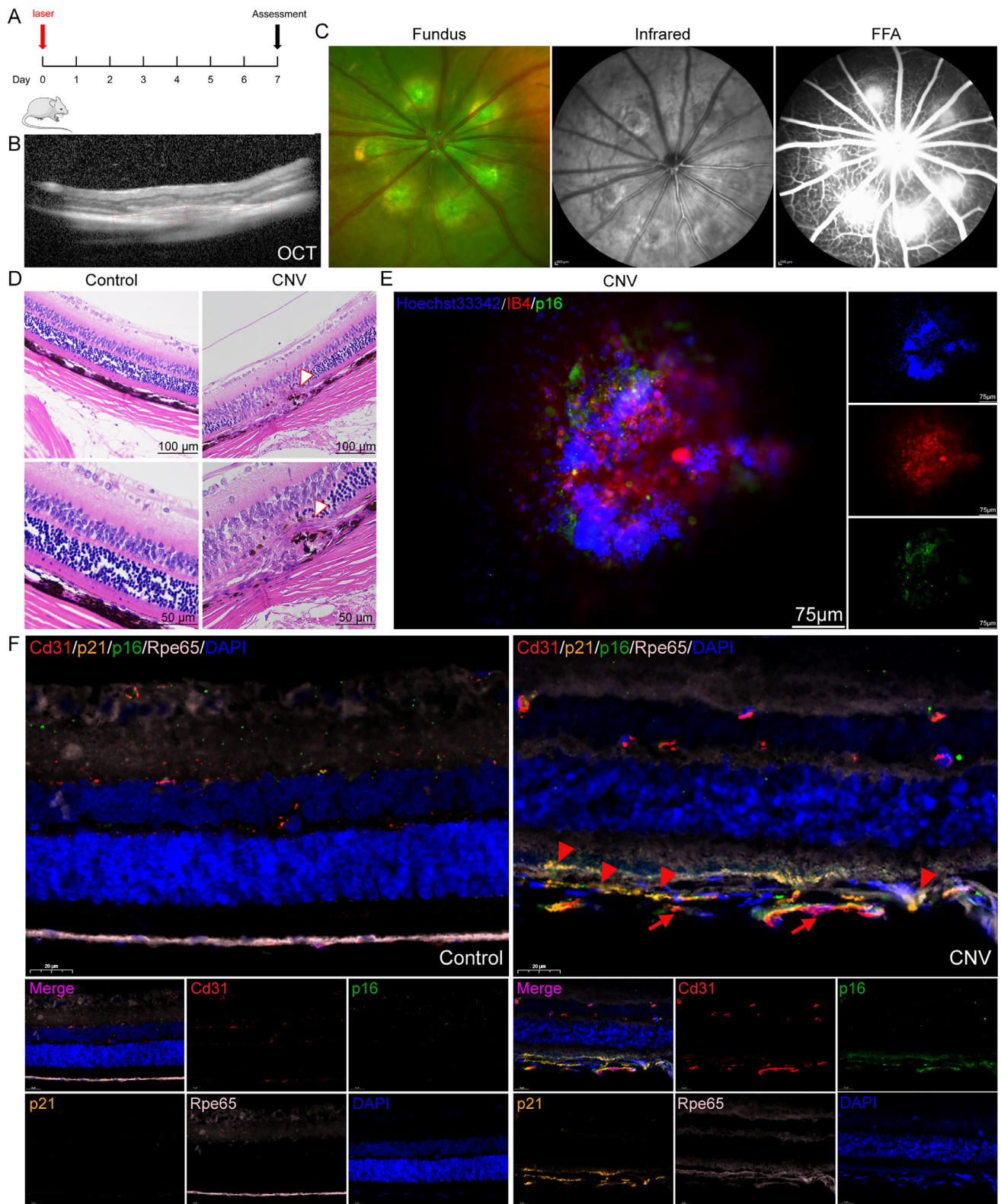
FIGURE 6. Laser-induced CNV rat model associated with senescent RPE cells. (**A**) Flowchart for the establishment of a laser-induced CNV rat model. (**B–D**) OCT (**B**), fundus photograph, infrared image, and FFA image (**C**), and H&E staining (**D**) of laser spots in the laser-induced CNV rat model. *Arrowheads* indicate the CNV lesion. (**E**) Immunofluorescence staining of IB4 and p16 for the RPE-choroid-sclera complex mount. (**F**) Multicolor immunofluorescent staining for p21, p16, Rpe65, and Cd31. *Arrowheads* indicate senescent RPE cells, and arrows indicate the CNV. OCT, optical coherence tomography.
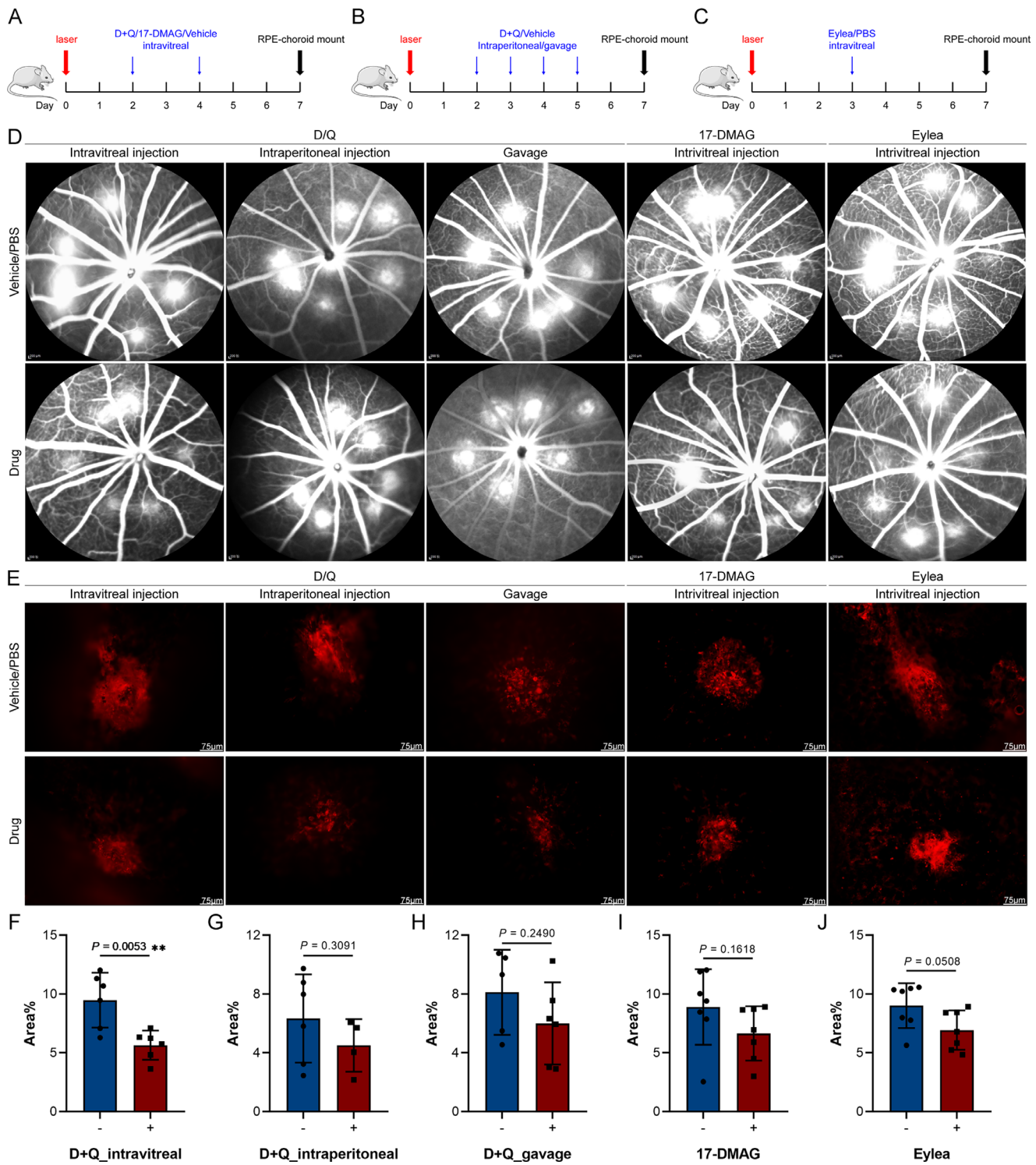
FIGURE 7. Intravitreal injection of senolytic drugs significantly alleviated the CNV. (**A–C**) Flowcharts for treatments with senolytic drugs (**A–B**) and aflibercept (**C**) in the laser-induced CNV rat model. (**D**) FFA of laser-induced CNV rats after treatment with D+Q, 17-DMAG, or aflibercept. (**E**) Immunofluorescence staining of the RPE-choroid-sclera complex mounts after treatment with D+Q, 17-DMAG, or aflibercept. (**F**) IB4$^+$ areas in the RPE–choroid–sclera complex mounts after intravitreal injection of D+Q ($n = 6$ without vs. $n = 6$ with D+Q). (**G**) IB4$^+$ areas in the RPE–choroid–sclera complex mounts after intraperitoneal injection of D+Q ($n = 6$ without vs. $n = 4$ with D+Q). (**H**) IB4$^+$ areas in the RPE–choroid–sclera complex mounts after gavage with D+Q ($n = 5$ without vs. $n = 6$ with D+Q). (**I**) IB4$^+$ areas in the RPE–choroid–sclera complex mounts after intravitreal injection of 17-DMAG ($n = 7$ without vs. $n = 7$ with 17-DMAG). (**J**) IB4$^+$ areas in the RPE–choroid–sclera complex mounts after intravitreal injection of aflibercept ($n = 7$ without vs. $n = 7$ with aflibercept). Each datapoint represents the average value of the lesions from one eye. *$P < 0.05$. The Student t test was used for comparisons between the two groups.
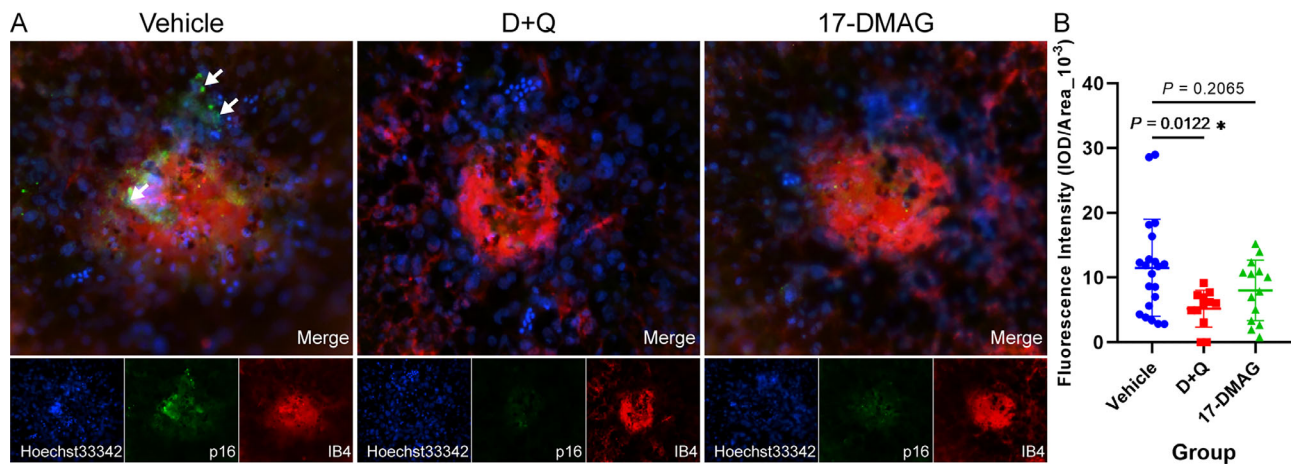
FIGURE 8. Intravitreal injection of senolytic drugs reduced the expression of p16 in CNV lesions. (**A**) Immunofluorescence staining of IB4 and p16 for RPE–choroid–scleral complex mount after intravitreal injection of senolytics. (**B**) Fluorescence intensity for p16 in CNV lesions after intravitreal injection of senolytics/ Vehicle: $n = 21$, D+Q: $n = 12$, 17-DMAG: $n = 14$; each datapoint represents 1 laser spot. *$P < 0.05$. One-way ANOVA was used for comparisons between groups.

In 17-DMAG–treated senescent ARPE-19 cells, Bax expression significantly increased without a reduction in Bcl-2 expression (Supplementary Figs. S5A, E, F). Cleaved caspase-3 levels were maintained in both senolytic groups (Supplementary Figs. S5A, G). These results indicate that senolytics (D+Q and 17-DMAG) induce apoptosis in senescent ARPE-19 cells via the Bcl-2/Bax system. As p62 levels were significantly reduced after treatment with D+Q (Supplementary Figs. S5A–B), the activated autophagy may play a role in the death of senescent ARPE-19 cells in this situation.

The Laser-Induced CNV Rat Model was Associated With Increased Senescence of RPE Cells

To explore the effects of senescence on neovascularization in vivo, we established a laser-induced CNV rat model (Fig. 6A). Optical coherence tomography, FFA, H&E staining, and RPE–choroid mounting showed that CNV was successfully established by the laser (Figs. 6B–E). We found that p16 was expressed in cells around the laser spot, confirming the presence of senescent cells in the laser-induced CNV rat models (Fig. 6E). To confirm the presence of senescent RPE cells, we conducted multicolor immunofluorescence staining for p21, p16, RPE, and CD31. Above the Cd31$^+$ area, the costaining of p21, p16, and RPE65 was higher than that in the control (Fig. 6F).

Senolytics Alleviated the Formation of CNV by Eliminating Senescent Cells

Senescent ARPE-19 cells are more sensitive to D+Q; therefore, agent this was used first to treat CNV. Using the "hit and run" strategy, we intraperitoneally administered D+Q as it has been systematically used in the past (Supplementary Fig. S6A). On day 7, the intensity and area of leakage of the laser points were significantly lower after D+Q administration (Supplementary Fig. S6B). On day 14, the leakage intensities of the laser points were similar in the D+Q and vehicle groups, whereas the area was slightly smaller in the D+Q group (Supplementary Fig. S6B); we then performed RPE–choroid mounting and found that the CNV area was significantly smaller after treatment with D+Q (Supplemen-

tary Figs. S6C–D). These results indicate that D+Q alleviated CNV progression.

The existence of the blood–retinal barrier prevents toxic substances and drugs from entering the eyes. Therefore, the route of intraocular diseases is important. In this study, we explored a suitable administration route for D+Q (Figs. 7A–B). FFA and RPE–choroid mounts indicated that the intravitreal administration of D+Q was the most suitable method for reducing the CNV area (Figs. 7D–H). We also evaluated the effect of 17-DMAG on CNV (Fig. 7A), observing that it only slightly alleviated CNV (Figs. 7D–E and I). This result indicates that the therapeutic effect of 17-DMAG was inferior to that of D+Q. Currently, intravitreal anti-VEGF therapy is the most common treatment for CNV and wAMD[4,25–27]; therefore, we investigated its effects on CNV in a rat model. Like the senolytics, aflibercept significantly reduced the degree of CNV (Figs. 7D–E and 7J).

To explore the senescent burden after treatment with senolytics, we conducted immunofluorescence staining for p16 using RPE–choroid–sclera complex mounts. After treatment with D+Q, the expression of p16 was significantly lower than that after treatment with the vehicle (Figs. 8A–B). The expression of p16 in the 17-DMAG group reduced without significance (Figs. 8A–B), consistent with the results of the in vitro assay.

DISCUSSION

Because wAMD is greatly vision threatening, and only 25% to 35% of patients with wAMD gain significant improvement in vision after regular anti-VEGF therapy,[28,29] various studies have focused on novel therapies for wAMD or CNV. Previous studies demonstrate that senescent RPE cells are associated with both dry and wAMD.[7] However, the effects of eliminating senescent RPE cells on CNV progression using various senolytic and transgenic methods have not been thoroughly investigated. Here, we explored the association between senescence and AMD using RNA-seq analysis, and investigated the effects of RPE cells on neovascularization both in vitro and in vivo.

Based on the bulk RNA-seq analysis, we found that senescence-associated genes in the RPE–choroid complex were significantly enriched in CNV lesions, accompanied by

accelerated angiogenesis and inflammation. Senescent cells can produce sets of proinflammatory factors—including IL-1, IL-6, IL-8, TNF-α, and VEGF—that subsequently cause inflammation and angiogenesis.[5,12] These results suggest that cellular senescence in the RPE–choroid may be associated with the activation of inflammation and angiogenesis, which promotes CNV or wAMD progression. Single-cell RNA-seq revealed that senescence-associated genes were expressed in multiple cell types in the RPE–choroid layer, suggesting that AMD is related to senescence of the entire retina. It has been reported that multiple types of retinal cells are senescent in individuals with AMD and elderly populations,[12] which is consistent with our results.

Next, senescence was induced in ARPE-19 cells using two methods. Senescent cells produce a set of SASPs—including proinflammatory cytokines, chemokines, growth factors, and MMPs—that are associated with chronic inflammation, epithelial-to-mesenchymal transition, and angiogenesis, and accelerate disease progression.[30] We observed the expression of SASPs in senescent APRE-19 cells, which can cause tissue dysfunction and inflammation.[31] Additionally, VEGF, the most important angiogenic factor, was upregulated in senescent ARPE-19 cells. These results were consistent with those of a previous study.[32] Inflammation—including inflammatory cytokines, complement system activation, and macrophage/microglia regulation—is thought to contribute to the formation of pathological neovascularization in AMD.[33,34] Thus, SASPs expressed by senescent cells in AMD may accelerate CNV progression through VEGF and inflammation. Intravitreal anti-VEGF therapy is the standard treatment for wAMD.[35] Nevertheless, it cannot reduce the production of VEGF or eliminate senescent cells that produce SASPs, making CNV persistent. Many patients experience an incomplete or no response to this treatment after repeated injections of anti-VEGF drugs,[4] supporting our view.

We further validated the effects of senescent ARPE-19 cells on ECs. Senescent ARPE-19 cells promoted the proliferation, migration, and invasion of HUVECs. Both dry AMD and wAMD are characterized by the dysfunction and/or death of all components of the photoreceptor–RPE–Bruch's membrane–choroid complex, because they are functionally integrated.[5] In wAMD, pathological neovascularization induced by angiogenic or proinflammatory factors, such as VEGF, penetrates Bruch's membrane, finally forming CNV.[5] Senescent RPE cells may promote this process, which is similar to the results of the migration and invasion assays in our study. Cao et al.[36] showed that senescent human fetal RPE cells induced by amyloid-β–secreted higher levels of MMP-9 than their nonsenescent counterparts. Consistently, the expression of MMP-3 was upregulated in senescent ARPE-19 cells. MMP-3 and/or MMP-9 released by senescent RPE cells may lyse tight junction proteins in the outer blood–retinal barrier, leading to their breakdown. Breakdown of the outer blood–retinal barrier probably assists in the penetration (migration or invasion) of ECs through Bruch's membrane, subsequently accelerating the progression of CNV or advanced AMD. Interestingly, young ARPE-19 cells slightly improved migration and invasion of HUVECs. An intact Bruch's membrane may prevent "normal" contact between RPE and choroidal ECs such that RPE may induce EC function under any contact conditions; still, RPE senescence may further induce EC functions.

Senolytic drugs alleviate several disorders in age-related mouse disease models, and significantly prolong the lifespan of aging mice.[14,37] D+Q and 17-DMAG, two types of senolytics that target different mechanisms, were shown to reduce various types of senescent cells in vitro and in vivo without destroying young cells, such as preadipocytes and murine embryonic fibroblasts.[23,24] In our study, we found that these two senolytics accelerated apoptosis in senescent ARPE-19 cells through a Bcl-2/Bax–associated mechanism. Interestingly, senescent ARPE-19 cells were more sensitive to D+Q treatment. The use of senolytic drugs—especially D+Q—to reduce senescent RPE cell abundance in vivo is promising. Cleaved caspase-3 levels were maintained in both senolytic groups. Additionally, as p62 was significantly reduced, we concluded that activated autophagy may participate in senescent ARPE-19 cell death. Similar stressors can induce autophagy or apoptosis, both of which inhibit each other. Although autophagy allows cells to adapt to stress and inhibits apoptosis, massive autophagy can kill cells and trigger apoptosis.[38] Therefore, the exact effect of autophagy on senescent ARPE-19 cell death after treatment of D+Q requires further investigation.

Here, we observed that D+Q and 17-DMAG alleviated the progression of laser-induced CNV, particularly after intravitreal injection. Additionally, intravitreal injection of D+Q was similar to that of aflibercept, suggesting that the elimination of senescent cells in vivo suppressed pathological neovascularization. A previous study reported that nutlin3a, a senolytic, could suppress CNV by reducing the senescent cell burden.[7] This finding is consistent with our results; however, nutlin3a was also reported to induce cell senescence.[8,9] Therefore, we used two types of senolytics to validate the role of senescent cells in CNV. Senolytic treatment promoted the apoptosis of senescent ARPE-19 cells, suggesting that senolytic therapy may induce dry AMD or geographic atrophy. Senomorphic factors in CNV or AMD—such as rapamycin and metformin[39]—thus require further investigation. A clinical case control study was conducted on metformin use for AMD, reporting that it was associated with reduced odds of developing AMD.[40] Furthermore, we used a transgenic mouse model to specifically eliminate senescent cells, observing that the degree of CNV had significantly decreased. This finding supports that senescent RPE cell-targeting therapy has great potential for treating CNV or wAMD.

This study had some limitations; first, the mechanisms underlying senescent cell-induced CNV have rarely been explored and require further investigation. Second, we did not validate the effects of senescent RPE cells on CNV in different species. Third, owing to the difference in vehicles, we did not directly compare the efficacy of senolytics with anti-VEGF therapy; thus, the clinical translation of senolytics in AMD requires further study. Fourth, primary human RPE (hRPE) and choroidal vascular ECs differ from ARPE-19 cells and HUVECs; therefore, it is better to conduct in vitro experiments using hRPE and choroidal vascular ECs. Nevertheless, owing to the inaccessibility of hRPE–choroid complexes in our hospital, it was difficult to obtain primary cultures of hRPE and choroidal vascular ECs. Moreover, three-dimensional CNV images are considerably more predictive than two-dimensional images, which is a limitation.

In conclusion, this study validated that senescent RPE cells could accelerate pathological neovascularization, and provided evidence supporting senescent cell-targeting therapy for CNV and wAMD.

Disclosure: **Y. Wang**, None; **Y. Tseng**, None; **Keyu Chen**, None; **Kuangqi Chen**, None; **Kai Chen**, None; **Z. Huang**, None; **Z. Mao**, None; **X. Li**, None

References

1. Finger RP, Fimmers R, Holz FG, Scholl HP. Incidence of blindness and severe visual impairment in Germany: projections for 2030. *Invest Ophthalmol Vis Sci*. 2011;52(7):4381–4389.
2. Rahman F, Zekite A, Bunce C, Jayaram H, Flanagan D. Recent trends in vision impairment certifications in England and Wales. *Eye (Lond)*. 2020;34(7):1271–1278.
3. Fleckenstein M, Keenan TDL, Guymer RH, et al. Age-related macular degeneration. *Nat Rev Dis Primers*. 2021;7(1):31.
4. Mettu PS, Allingham MJ, Cousins SW. Incomplete response to Anti-VEGF therapy in neovascular AMD: exploring disease mechanisms and therapeutic opportunities. *Prog Retin Eye Res*. 2021;82:100906.
5. Blasiak J. Senescence in the pathogenesis of age-related macular degeneration. *Cell Mol Life Sci*. 2020;77(5):789–805.
6. Lee KS, Lin S, Copland DA, Dick AD, Liu J. Cellular senescence in the aging retina and developments of senotherapies for age-related macular degeneration. *J Neuroinflammation*. 2021;18(1):32.
7. Chae JB, Jang H, Son C, et al. Targeting senescent retinal pigment epithelial cells facilitates retinal regeneration in mouse models of age-related macular degeneration. *Geroscience*. 2021;43(6):2809–2833.
8. Vilgelm AE, Pawlikowski JS, Liu Y, et al. Mdm2 and aurora kinase a inhibitors synergize to block melanoma growth by driving apoptosis and immune clearance of tumor cells. *Cancer Res*. 2015;75(1):181–193.
9. Xu X, Liu Q, Zhang C, et al. Inhibition of DYRK1A-EGFR axis by p53-MDM2 cascade mediates the induction of cellular senescence. *Cell Death Dis*. 2019;10(4):282.
10. Hayflick L, Moorhead PS. The serial cultivation of human diploid cell strains. *Exp Cell Res*. 1961;25:585–621.
11. van Deursen JM. The role of senescent cells in ageing. *Nature*. 2014;509(7501):439–446.
12. López-Luppo M, Catita J, Ramos D, et al. Cellular senescence is associated with human retinal microaneurysm formation during aging. *Invest Ophthalmol Vis Sci*. 2017;58(7):2832–2842.
13. Mishima K, Handa JT, Aotaki-Keen A, Lutty GA, Morse LS, Hjelmeland LM. Senescence-associated beta-galactosidase histochemistry for the primate eye. *Invest Ophthalmol Vis Sci*. 1999;40(7):1590–1593.
14. Kirkland JL, Tchkonia T. Senolytic drugs: from discovery to translation. *J Intern Med*. 2020;288(5):518–536.
15. Saccon TD, Nagpal R, Yadav H, et al. Senolytic combination of dasatinib and quercetin alleviates intestinal senescence and inflammation and modulates the gut microbiome in aged mice. *J Gerontol A Biol Sci Med Sci*. 2021;76(11):1895–1905.
16. Wang L, Wang B, Gasek NS, et al. Targeting p21(Cip1) highly expressing cells in adipose tissue alleviates insulin resistance in obesity. *Cell Metab*. 2022;34(1):75–89.e8.
17. Oubaha M, Miloudi K, Dejda A, et al. Senescence-associated secretory phenotype contributes to pathological angiogenesis in retinopathy. *Sci Transl Med*. 2016;8(362):362ra144.
18. Campos M, Amaral J, Becerra SP, Fariss RN. A novel imaging technique for experimental choroidal neovascularization. *Invest Ophthalmol Vis Sci*. 2006;47(12):5163–5170.
19. Baker DJ, Wijshake T, Tchkonia T, et al. Clearance of p16Ink4a-positive senescent cells delays ageing-associated disorders. *Nature*. 2011;479(7372):232–236.
20. Zhang L, Tong X, Huang J, et al. Fisetin alleviated bleomycin-induced pulmonary fibrosis partly by rescuing alveolar epithelial cells from senescence. *Front Pharmacol*. 2020;11:553690.
21. Zhong J, Chen J, Oyekan AA, et al. Ionizing radiation induces disc annulus fibrosus senescence and matrix catabolism via MMP-mediated pathways. *Int J Mol Sci*. 2022;23(7):4014.
22. Hernandez-Segura A, Nehme J, Demaria M. Hallmarks of cellular senescence. *Trends Cell Biol*. 2018;28(6):436–453.
23. Fuhrmann-Stroissnigg H, Ling YY, Zhao J, et al. Identification of HSP90 inhibitors as a novel class of senolytics. *Nat Commun*. 2017;8(1):422.
24. Zhu Y, Tchkonia T, Pirtskhalava T, et al. The Achilles' heel of senescent cells: from transcriptome to senolytic drugs. *Aging Cell*. 2015;14(4):644–658.
25. Cheung CMG, Arnold JJ, Holz FG, et al. Myopic choroidal neovascularization: review, guidance, and consensus statement on management. *Ophthalmology*. 2017;124(11):1690–1711.
26. Sarwar S, Clearfield E, Soliman MK, et al. Aflibercept for neovascular age-related macular degeneration. *Cochrane Database Syst Rev*. 2016;2:CD011346.
27. Ohno-Matsui K, Ikuno Y, Lai TYY, Gemmy Cheung, CM. Diagnosis and treatment guideline for myopic choroidal neovascularization due to pathologic myopia. *Prog Retin Eye Res*. 2018;63:92–106.
28. Dugel PU, Koh A, Ogura Y, et al. HAWK and HARRIER: phase 3, multicenter, randomized, double-masked trials of brolucizumab for neovascular age-related macular degeneration. *Ophthalmology*. 2020;127(1):72–84.
29. Martin DF, Maguire MG, Ying GS, Grunwald JE, Fine SL, Jaffe GJ. Ranibizumab and bevacizumab for neovascular age-related macular degeneration. *N Engl J Med*. 2011;364(20):1897–1908.
30. Campisi J. Aging, cellular senescence, and cancer. *Annu Rev Physiol*. 2013;75:685–705.
31. Birch J, Gil J. Senescence and the SASP: many therapeutic avenues. *Genes Dev*. 2020;34(23-24):1565–1576.
32. Sreekumar PG, Reddy ST, Hinton DR, Kannan R. Mechanisms of RPE senescence and potential role of αB crystallin peptide as a senolytic agent in experimental AMD. *Exp Eye Res*. 2022;215:108918.
33. Tan W, Zou J, Yoshida S, Jiang B, Zhou Y. The role of inflammation in age-related macular degeneration. *Int J Biol Sci*. 2020;16(15):2989–3001.
34. Ishikawa K, Kannan R, Hinton DR. Molecular mechanisms of subretinal fibrosis in age-related macular degeneration. *Exp Eye Res*. 2016;142:19–25.

35. Ricci F, Bandello F, Navarra P, Staurenghi G, Stumpp M, Zarbin M. Neovascular age-related macular degeneration: therapeutic management and new-upcoming approaches. *Int J Mol Sci*. 2020;21(21):8242.

36. Cao L, Wang H, Wang F, Xu D, Liu F, Liu C. Aβ-induced senescent retinal pigment epithelial cells create a proinflammatory microenvironment in AMD. *Invest Ophthalmol Vis Sci*. 2013;54(5):3738–3750.

37. Tchkonia T, Kirkland JL. Aging, cell senescence, and chronic disease: emerging therapeutic strategies. *JAMA*. 2018;320(13):1319–1320.

38. Maiuri MC, Zalckvar E, Kimchi A, Kroemer G. Self-eating and self-killing: crosstalk between autophagy and apoptosis. *Nat Rev Mol Cell Biol*. 2007;8(9):741–752.

39. Di Micco R, Krizhanovsky V, Baker D, d'Adda di Fagagna F. Cellular senescence in ageing: from mechanisms to therapeutic opportunities. *Nat Rev Mol Cell Biol*. 2021;22(2):75–95.

40. Blitzer AL, Ham SA, Colby KA, Skondra D. Association of metformin use with age-related macular degeneration: a case-control study. *JAMA Ophthalmol*. 2021;139(3):302–309.